Original Article

Institution of MECHANICAL ENGINEERS
Journal of AEROSPACE ENGINEERING

Proc IMechE Part G:
J Aerospace Engineering
0(0) 1–18

DOI: 10.1177/0954410017724821
journals.sagepub.com/home/pig
SAGE

# Intelligent attitude planning algorithm based on the characteristics of low radar cross section characteristics of microsatellites under complex constraints

**Bing Hua[1], Rui-Peng Liu[1], Yun-Hua Wu[1] and Da-Fu Xu[2]**

**Abstract**

The attitude optimization problem of spacecraft under restricted conditions is an important issue of spacecraft planning control. This paper aims at on-orbit microsatellites, which is based on the directional characteristics of their own low radar cross section designs, maintaining low detection probabilities for ground, sea, and space-based detection systems, and simultaneously satisfying the constraint conditions of complex attitude constraints. In this paper, an improved pigeon-inspired optimization algorithm and a nonredundant attitude description method—modified Rodrigues parameters—are used to solve the problem of attitude optimal planning for satellites under complex constraints. This paper focuses on the core evolution mathematical model of the pigeon-inspired optimization algorithm based on the modified Rodrigues parameter, the iterative evolution process of the individual in the pigeon population, and the fitness function model of the individual at different positions. The comparison between the classical pigeon-inspired optimization algorithm and the improved pigeon-inspired optimization algorithm is made in the planned result and resource occupancy, respectively. The simulation results show that the improved algorithm has a faster convergence speed and a smoother optimization result than the classic pigeon-inspired optimization algorithm, where it greatly reduces the computational load and reduces the load of the control system, thus achieving an optimal algorithm.

**Keywords**

Attitude planning, complex constraint conditions, low radar cross section characteristics, pigeon-inspired optimization algorithm, modified Rodrigues parameter

Date received: 25 January 2017; accepted: 12 July 2017

## Introduction

Microsatellites have the characteristics of simple structure, small volume, light weight, low cost, fast assembling, and so on, and because it is based on the advantage of volume and quality, it can recognize the rapid deployment of a large number of satellites, which has a crucial position in military and civil fields. However, due to its size and quality limitations, satellite fuel has certain constraints, and the large attitude changes result in the consumption of large amounts of fuel, greatly reducing the service life of the satellite. At the same time, in-orbit satellites are also vulnerable for a variety of anti-satellite radar detection equipments.

With the rapid development of space anti-satellite technology, the United States and Russia have the most advanced space surveillance system with strategic missile monitoring functions.[1] The greatest threats to microsatellites are the ground-based radar, sea-based radar, space-based radar, infrared, and optical monitoring system, which range from hundreds of kilometers to thousands of kilometers, and some up to tens of thousands of kilometers. At present, the United States has a larger, more advanced global space exploration system. The system consists of Naval Space Surveillance System (NAVSPASUR),[2] Space Tracking System (STS), Ground-based Electro-optical Deep Space Surveillance (GEODSS), Space-based Surveillance System (SBSS) and others. Space detection of phased array radar, synthetic aperture radar, optical

[1]Micro-Satellite Engineering Technology Research Center, College of Astronautics, Nanjing University of Aeronautics and Astronautics, Jiangsu, China
[2]Aerospace System Engineering, Shanghai, China

**Corresponding author:**
Bing Hua, College of Astronautics, Nanjing University of Aeronautics and Astronautics, Yudao Street 29, Nanjing, Jiangsu 210016, China.
Email: huabing@nuaa.edu.cn

detection equipment and also HAX radar works in the Ku band with the center frequency of 16 GHz and bandwidth of 2 GHz, and can detect the target where the orbital height is less than 6400 km and the diameter is greater than 1 $cm^1$ accurately positioned to track the target diameter of 10 cm. In the geosynchronous orbit, it can be achieved with a precise positioning and tracking the target of 30 $cm^3$ diameter.

In recent years, with the rapid development of space detection equipment and anti-satellite weapons, the technology of low detectability has also developed rapidly. Effective technical measures can be used to attenuate (or eliminate) the satellite's radar, laser, visible, and infrared scattering characteristics and make satellite functions and operational intentions hard (or unable) to be identified,[4] which is prominently present. The space-based detection equipment is based on the observability of the target, therefore, the key to improving the operational efficiency and survivability of on-orbit satellites using low-detectability technology is to reduce the detectability of space exploration equipment and anti-satellite weapons to astronomical objects. In terms of microsatellite stealth technology, the design of radar cross section (RCS) is the most simple and effective way to increase the difficulty of radar detection.[5]

However, one of the important aspect of the stealth fighter is the satellite stealth technology, which is usually based on a certain shape structure, and this structure has extremely clear directionality. Therefore, the attitude planning results based on the azimuth and pitch angles of the radar will directly determine the stealth performance and effect of the satellite.

At present, for the spacecraft attitude planning problem, the constraint monitoring algorithm of the ''Cassini'' Saturn probe[6] and the planning method of the path bypassing proposed by Hablani achieved the spacecraft attitude movement of the autonomous real-time planning, but this algorithm cannot optimize the path with target.[7] Avanzini et al.[8] constructed the potential function such that the attitude can move toward the potential function, so as to achieve the attitude planning and attitude avoidance, but the problem brought to this method is easy to fall into the local optimal solution. Kim and Mesbahi[9] considered the dynamics and spatial geometric constraints together to transform the attitude planning problem into semi-definite programming problem, but the algorithm will increase dramatically as the constraint increases.

At present, the problem of low detectability attitude planning for microsatellites has not been published at inland and abroad except that of Su and Zhou.[10] However, the current attitude-planning algorithm only considers the threat posed by the exploratory radar to the satellite, and does not consider the satellite's own payload and the task's limitation on the satellite attitude. Meanwhile, the current research does not plan the rolling angle of the satellite, and because only the threat of the sea-based radar is considered, the pitch angle of the attitude planning algorithm can only be planned in [0–180°].

Based on the limitations of microsatellites' quality, volume and attitude control ability, and the development of space-based space exploration technology, this paper will discuss the three-axis omnidirectional attitude planning algorithm, so that the attitude of a satellite can be a safe, convenient, low power to avoid the attitude of the path to the restricted area, while maintaining a low detectability.

The paper is organized as follows: the upcoming section introduces the low RCS structure based on on-orbit microsatellites. Next section introduces the modified Rodrigues parameter and the attitude space under the modified Rodrigues parameter. Subsequent section introduces the classical PIO algorithm and its fitness function model and the improved PIO algorithm and its fitness function model. Finally, the experimental results of two different algorithms are introduced and conclusions are provided.

## Problem establishment

The orbital height of microsatellites is low, generally in hundreds of kilometers of altitude. The main threat to microsatellites comes from detection systems consisting of ground-based, sea-based, and space-based radars.[7] The orbit of stars can be calculated by the detection of microsatellite tracking and, thus, the next over-location and time can be accurately forecasted. When combined with appropriate interference and camouflage, it can also reduce the satellite's performance effectively. The microsatellite must then maintain a specific attitude angle for the radar detection, beam based on its own with low RCS structure.

If satellites are about to enter the ground, sea-based, and space exploration radar detection area, the attitude planning of the low RCS structure of the satellite must be carried out when the satellite crosses the threat zone according to the characteristics of the threat radar distribution coordination, radar's power, pitch angle, and wave band. So that the low RCS structure of the satellite is always aligned with the weighted detection center of the ground-based, space-based detection system to achieve the lowest detectability. As shown in Figure 1, from satellite No. 1 (the satellite being detected) to the ground lead tangent, from each tangent will form a cone. Ground radars R1, R2, R3 in the CDB arc and space detection radars mounted on the satellite No. 2 (space-based detection satellite) will threaten satellite No. 1, the radars R4, R5, R6 in the CEB arc do not pose a threat, and with the movement of the satellite, the threat from the space radar and R1 will gradually weaken to disappear. With the R6 radar gradually into the horizon, the threat of radar to satellite No. 2 will gradually increase; satellite No. 2 should be followed with the corresponding attitude

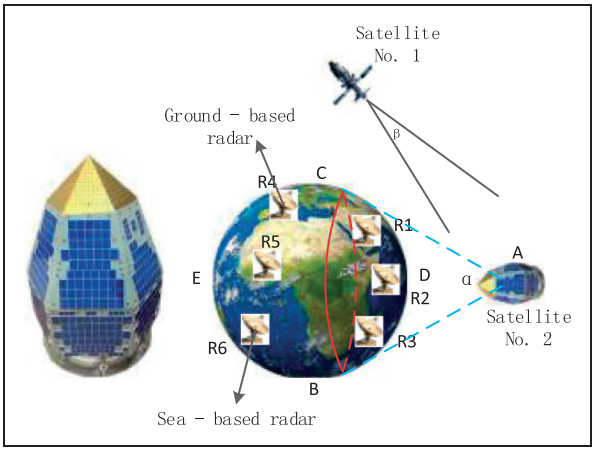


**Figure 1.** Low RCS structure design and space configuration of "Tianxun number one".

adjustment. And the satellite payload and the task will pose a constraint on the satellite attitude and requirements. Assuming the satellite is a remote sensing satellite, the CCD camera on the satellite will burn the charge-coupled device if it is pointing at the sun for a long time during the gesture planning process. Based on the above two factors, this paper focuses on the problem of attitude optimal programming for microsatellites under the condition of a series of complex attitude constraints and attitude requirements.

## The establishment of attitude space based on modified Rodrigues parameter

### *Modified Rodrigues parameter space*

The currently used methods of describing satellite attitude are the Euler angle, direction cosine method, and quaternion method. Euler angles are a set of minimum implementations of describing gestures, but the operation of trigonometric functions and inverse trigonometric functions are too much to compute. Directional cosine method needs to solve nine equations but the computational complexity is still large. Quaternion method has only one redundancy, it only needs to solve four equations, when compared to the previous two methods with regard to the computation and its complexity has been greatly improved, but because of its redundancy, its covariance matrix comes into being singular, which affects its application effect. While the modified Rodrigues parameter does not need trigonometric function or iterative calculation, and the computational efficiency is about one time better than the quaternion method.[8,9] There are no restrictions on the angle, no redundant constraints, and it can be directly used as attitude error signal for attitude control. The usage of the modified Rodrigues parameter as the control signal only needs a linear feedback control that can easily achieve a wide range of asymptotic convergences.

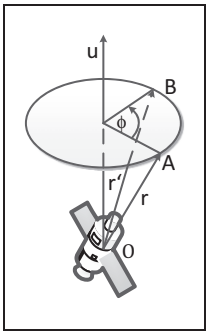


**Figure 2.** The modified Rodrigues parameters of satellite rotation.

In the modified Rodrigues parameter coordinate system (hereinafter referred to as R coordinate system), the $x$-axis of the satellite at the initial moment is located at the vector $OA = r$, and is located at $OB = r'$ after the elapse of time $t$. The rotation is equivalent to the satellite with regard to the unit vector $u$ as the axis of rotation, and rotate by $\phi$ degrees. The rotation angle $\phi$ and the unit vector $u$ can be expressed in the form of $u\phi$, denoted by $\Phi$ called the modified Rodrigues parameter (hereinafter referred to as R-parameter) (Figure 2).

$$\Phi = \tan\left(\frac{\varphi}{4}\right) * u \tag{1}$$

And irrespective of its clockwise or counterclockwise rotations of more than 180°, it can be equivalent to the opposite direction of rotation $|\varphi|$. After the R-parameter is obtained, it can be expressed as a vector form $\Phi = \begin{bmatrix}\sigma_1 & \sigma_2 & \sigma_3\end{bmatrix}^T$, and the attitude matrix $A$ is obtained

$$\mathbf{A} = \frac{1}{(2-\sum)^2}\begin{bmatrix} \sum^2 + 4(\sigma_1^2 - \sigma_2^2 - \sigma_3^2) & 8\sigma_1\sigma_2 - 4\sum\sigma_3 & 8\sigma_1\sigma_3 + 4\sum\sigma_2 \\ 8\sigma_1\sigma_2 + 4\sum\sigma_3 & \sum^2 + 4(\sigma_2^2 - \sigma_1^2 - \sigma_3^2) & 8\sigma_2\sigma_3 - 4\sum\sigma_1 \\ 8\sigma_1\sigma_3 - 4\sum\sigma_2 & 8\sigma_2\sigma_3 + 4\sum\sigma_1 & \sum^2 + 4(\sigma_3^2 - \sigma_1^2 - \sigma_2^2) \end{bmatrix} \tag{2}$$

where $\sum = 1 - (\sigma_1^2 + \sigma_2^2 + \sigma_3^2)$, and has the following definition

$$A = \begin{bmatrix} T_{11} & T_{12} & T_{13} \\ T_{21} & T_{22} & T_{23} \\ T_{31} & T_{32} & T_{33} \end{bmatrix}$$

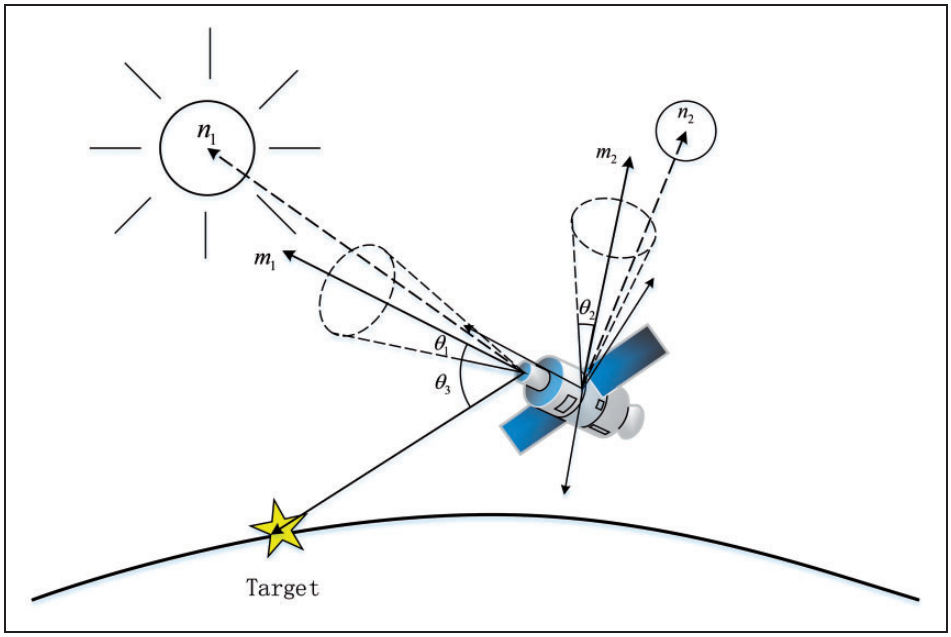


**Figure 3.** Microsatellite space avoidance and restricted attitude.

Thus, the pitch angle $\theta$, the roll angle $\gamma$, and the yaw angle $\psi$ can be expressed as

$$\begin{cases} \theta = \arcsin(T_{32}) \\ \gamma = \arctan\left(-\frac{T_{31}}{T_{33}}\right) \\ \psi = \arctan\left(\frac{T_{12}}{T_{22}}\right) \end{cases} \tag{3}$$

## *Establishment of attitude planning spatial model*

The attitude space coordinate system consists of three mutual orthogonal pitch axes, the yaw axis, and the roll axis as shown in Figure 4.

The attitude space is constructed with regard to the modified Rodrigues parameter space. The three axes of the space are three elements of the R-parameter vector. Meanwhile, it has to be taken into account the spacecraft in orbit to avoid some dangerous points: e.g.[19] low-temperature cooling telescope cannot be pointed at the sun; the star sensor cannot be pointed at the sun or other bright areas; heat dissipation surface cannot be exposed to the sun's radiation for a long time as shown in Figure 3.

There are two constraints in the constraint model of attitude planning, i.e. prohibiting entry into the area and prohibiting the exit from the area.[20] The microsatellite telescope and other optical sensitive devices's center view of the vector is as $m_i$, bright light objects relative to the direction of small satellites vector as $n_i$, the corresponding viewing angle as $\theta_i$, and it is required that the angle between optical sensors and light celestial bodies must be greater than a certain value (corresponding to the first constraint). At the same time, it is necessary that the relative angle of the optical remote sensing device of the satellite to the target must be smaller than the viewing angle of the device (corresponding to the second constraint) as well as constraints imposed by various other factors.

The attitude angle of the corresponding satellite above the limiting region is converted into R-parameter, corresponding to the R-parameter planning space as shown in Figure 4. In the R-parameter planning space, various restricted regions are corresponding to the sphere with a certain attitude as the center of the sphere, and if the constraint is nonspherical, then they are equalized as various spheres, and then these spheres are gathered together to make their outer envelope close to the corresponding restricted area.

In the R-parameter space, each of the gestures that need to be circumvented are as follows: the property of the threat source, and the threat level corresponding to the spherical coordinates of each sphere in the space, the radius of the sphere, and the threat level set for each sphere. And the area of the threat that needs to be avoided is positive and the threat level of the nondeparting area is negative. The R-parameter of the target attitude is set as $\Phi_t = [\sigma_1 \quad \sigma_2 \quad \sigma_3]^T$, which is based on the information of the azimuth of the ground, sea, and space radar.

Let the initial R-parameter be $\Phi_0 = \begin{bmatrix} 0 & 0 & 0 \end{bmatrix}^T$, based on the information of the orientation of the ground, sea-based, and space-based radar, combined with the low RCS directional characteristics of the microsatellite. The R-parameter of the target can be expressed as $\Phi_t = [\sigma_1 \quad \sigma_2 \quad \sigma_3]^T$, and at the same

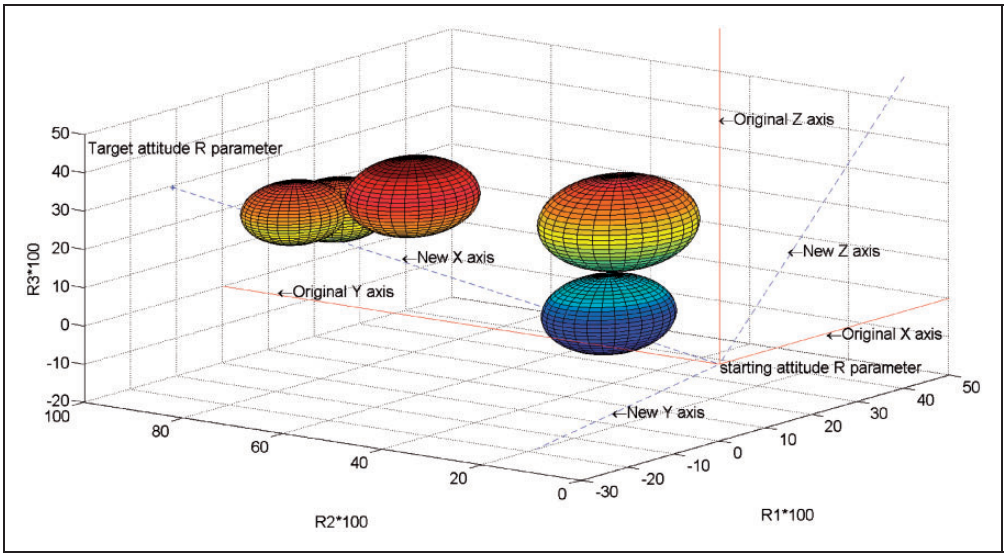


**Figure 4.** The R-parameter spatial representation of target attitude and restricted attitude.

time, the mission requirements of the microsatellite, payload constraints, and a series of attitude need to circumvent or restrict the conversion to the corresponding R-parameters. In the R-parameter space, each posture is to be restricted or evaded, where the nature of the threat source and the threat level correspond to the sphere coordinates of each sphere in the space, the radius of the sphere, and the threat level for each sphere, respectively.

At the same time, in order to simplify the model and reduce the computation, rotation is carried out in the $X$-axis (indicated by the solid red line in Figure 4) in the original R-parameter space to a direction that is the orientation of the starting attitude to the target attitude. The original $Y$-, $Z$-, and $X$-axis are fixed,[21] and rotate to get a new R-parameter space coordinate system (dashed blue line in Figure 4). In this paper, all the parameters, targets, and obstacles of the attitude space model are all established in the new R-parameter attitude space.

Assume that the initial attitude of the satellite in the R-parameter space is $\begin{bmatrix}\sigma_{1,0} & \sigma_{2,0} & \sigma_{3,0}\end{bmatrix}^T$, based on the low RCS characteristics of the satellites and the azimuth angle of the threat source, the planning target attitude of the satellite attitude is $\begin{bmatrix}\sigma_{1,d} & \sigma_{2,d} & \sigma_{3,d}\end{bmatrix}^T$. According to the payload and so on, the center of the threat region in the R-parameter space is $T_{center}(k) = \begin{bmatrix}\sigma_{1,T} & \sigma_{2,T} & \sigma_{3,T}\end{bmatrix}^T$, the radius of the threat area is $T_{radius}(k)$, and the threat level is $t_k$.

## Attitude planning algorithm based on improved pigeon-inspired optimization

In recent years, various population-based swarm intelligence algorithms have developed rapidly, and are widely used in various fields of dynamic programming optimization problem. The most notable of these are particle swarm optimization (PSO), ant colony optimization, artificial bee colony (ABC), and intelligent water drops (IWD). However, these algorithms have some problems such as slow convergence speed, easy to fall into local optimal solution, low computational efficiency, and long time in computer simulation. In view of the above problems, the classic PIO algorithm needs to achieve some improvement.

### *Classic PIO optimization algorithm*

Classic PIO algorithm is developed based on the pigeon in homing navigation process. When away from the destination, pigeons rely on the Earth's magnetic field and the location of the sun to navigate, and when they near their destination they mainly rely on some typical landmarks to navigate.[14] The pigeon population will produce elite individuals, which will lead the pigeons who are not familiar with the landmarks flying to the destination. Thus, the PIO optimization algorithm has two operators: (1) Map and compass operator, (2) Landmark operator, which respectively play the sun and the Earth's magnetic field and landmarks role in the planning process.[10]

*Map and compass operator.* In the R-parameter space, suppose $x_i$,$v_i$ be the position and velocity of the $i$-th individual. $x_p$, $x_g$ are respectively the optimal positions for each individual in the current iteration and the optimal position generated by all individuals in the current iteration, $M$ is the number of individuals, $T_1$, $T_{MAX}$, $T$ is the number of iterations of the map compass operator, maximum, and the current number of iterations. $D$ is the individual evolution dimension, $R$ is the map compass factor, which is a

fixed value between 0 and 1, *rand* is a random number between 0 and 1. The map and compass operator keeps each individual searching in nearby areas by iterating over and over to get a relatively ideal position and speed.[15,16] The evolution law can be expressed as follows

$$V(T+1) = V(T) + rand \times \left(x_p(T) - x(T)\right) \tag{4}$$

$$X(T+1) = X(T) \times \left(1 - e^{-RT}\right) + V(T+1) \tag{5}$$

*Landmark operator.* In nature when pigeons are adjacent to the destination, they switch landmarks as a guide to reach the destination, and those that are unfamiliar with the landmark, will follow pigeons familiar with the landmark. Similarly, the classic PIO algorithm will switch to the landmark operator after a certain number of map compass operators iterations to achieve rapid convergence and screening, retaining the elitists generated in previous iterations. The evolution of the law can be expressed as follows[10–12]

$$M(T+1) = \frac{M(T)}{2} \tag{6}$$

$$X_i(T+1) = X_i(T) + rand \times (X_C(T) - X_i(T)) \tag{7}$$

$$X_C(T) = \frac{\sum X_i(T) \cdot Fitness(X_i(T))}{M(T) \cdot \sum Fitness(X_i(T))} \tag{8}$$

where $M(T)$ is the number of individuals in the $T$th evolution and this value in each iteration is reduced by half in order to achieve the purpose of rapid convergence, $X_C(T)$ is the position of the current pigeons center, $Fitness(X_i(T))$ is the fitness value of the $i$th individual in the $T$th evolution. At this stage of the operator, the fitness values of each individual in the pigeon group are calculated after each iteration,[17,18] and the individuals whose fitness values are located at the latter half are removed from the target according to the order from small to large to achieve rapid screening thus retaining the purpose of the best individual.

## Improved PIO algorithm

Classic PIO, although possesses a fast convergence characteristics,[12,13] still has the probability of falling into the local optimal solution, and though the experimental data analysis is carried out, the variance of the planning result is large. This will let the satellite start the booster for attitude adjustment frequently; this is not allowed in the optimal control. In order to avoid the planning result fall into the local optimal solution, optimization planning results, further speeding up the convergence. This paper studied the planning process of classical PIO algorithm. Considering the communication between individuals during iteration process of evolution and the one individual's experience of the previous iterative process, the map and compass operator of the classic PIO algorithm has been modified, and the refinement and improvement of the fitness function model have been carried out.

After a large number of simulations, it is found that with the increasing number of the iterations, the map compass operator stage has already produced a part of the elite individuals. While in this part the classic PIO algorithm analyze each individual separately, in the process of evolution, only the evolution of each individual before the results as a reference is done, and in the evolution process, the classic PIO algorithm only reference the previous evolutionary results of each individual alone, but ignoring the learning of other individuals. And if the links strengthen between individuals at the map and compass operator stage, considering the impact of elite individuals on the whole group, it will make the whole pigeon group closer to the optimal solution with stronger directionality further speeding up the convergence rate.

The classic PIO algorithm allows the individual's speed to be the basis of the dynamic search range, if there is a local optimal solution in a relatively small area, and thereby it is possible to fall into the local optimum when the global optimal solution is relatively far away. To solve this problem, improved PIO algorithm adds an activation factor in the evolution, where the activator is activated when the entire population is relatively inactive, in the next period of time to increase the search scope of dynamic evolution so that the whole group can get away from the local optimal solution. And in order to avoid the activation factor from starting up frequently where the algorithm has already obtained the global optimal solution, it is set that if the fitness is not further reduced at the third activation, then the current solution is the global optimal solution. The activation factor is no longer activated in the iterations.

The improved PIO algorithm's map and compass operator is described as follows

$$\begin{aligned} V(T+1) = {} & inv \cdot V(T) + e_1 \cdot \left(\sigma_p - \sigma^i(T)\right) \\ & + e_2 \cdot \left(\sigma_g - \sigma^i(T)\right) \end{aligned} \tag{9}$$

$$\sigma(T+1) = \sigma(T) \times \left(1 - e^{-RT}\right) + V(T+1) \tag{10}$$

$$e_1 = \log_{T_1}^{T_1 - T} \tag{11}$$

$$e_2 = \log_{T_1}^{T} \tag{12}$$

$$inv \sim \left|N(0, \varepsilon)\right| \tag{13}$$

where $\sigma(T)$ and $V(T)$ denote the R-parameter representation of the three-axis angle and angular

velocity of the satellite evolved in the $T$th iteration, $\sigma_p$ and $\sigma_g$ are the local optimal evolution results of the individual before the current iteration and the global optimal evolution result of all individuals before the current iteration, $\sigma^i(T)$ denotes the R-parameter of the satellite attitude angle evolved by the $i$th individual in $T$ iteration, $inv$ is an absolute value function of a normal distribution with the mean of 0 and the variance of $\varepsilon$, changing the value of $\varepsilon$ controls the dynamic search range of pigeons, $e_1$ is the individual factor, which represents the recognition and learning from the local optimal result generated before the current iteration, $e_2$ is the communication factor and represents the individual's learning of the elite individual before the current iteration. The activation factor will be activated when the changing rate of the fitness value of the pigeons is less than 0.1, for 10 consecutive iterations. In the next 30 iterations, the activation factors variance is taken as $\varepsilon = \mathrm{d}t/\mathrm{d}f$, with a large dynamic search range to make groups out of the local optimal solution.

## Fitness function

The evolution function introduced in the previous section determines whether it can generate the individuals, which meet the optimization requirements, and the quality of the fitness function determines whether the algorithm can find out these outstanding individuals.

## Classic PIO fitness function

The fitness function of the classic PIO algorithm only uses the distance and the threat level as the criterion to evaluate the merits of the individual, in calculating the distance from the threat center, and the attitude planning results are equally divided into several small segments in R-parameter space. Let the distance from each segment to the threat center be the criterion for determining whether this segment is in the threat area. The fitness function of the $i$th individual is

$$Fitness(i) = w_1 \cdot distance(i) + w_2 \cdot threat(i) \tag{14}$$

$$diatance(i) = \sum_{j=0}^{n} L_{i,j} \tag{15}$$

$$threat(i) = \begin{cases} 0, & if\ R_{i,j} > R_j \\ \frac{L_{i,j}}{5} \sum_{k=1}^{N_t} t_k \left( \frac{1}{d_{0.1,k}^4} + \frac{1}{d_{0.3,k}^4} + \frac{1}{d_{0.5,k}^4} + \frac{1}{d_{0.7,k}^4} + \frac{1}{d_{0.9,k}^4} \right), & else \end{cases} \tag{16}$$

where$w_1$ and $w_2$ are the weight coefficients used to adjust the planning results to avoid obstacle priority or the shortest time priority, and $w_1 + w_2 = 1$. And $L_{i,j}$ is the length of the $j$th planning segment of the $i$ individual, $t_k$ is the threat level of the $k$th threat, $N_t$ is the number of threats, $d_{0.1,k}$ is the distance from the $k$th threat center to one-tenth of this planning segment, $R_j$ is the threat radius of the $j$th threat, $R_{i,j}$ is the mean distance from the $i$th planning segment to the $j$th threat center.[10]

*Modified PIO fitness function.* The fitness function of the classical PIO algorithm only takes the overall attitude planning distance and attitude, which at the threat region is taken into consideration, but not considering the characteristics of attitude at nonthreat region can still affect the overall planning effect of the algorithm and optimization effect. In the same area, fitness function establishes the different evaluation criteria for individuals with different location characteristics. Not only can refine the evaluation and prevent misjudgment, make the algorithm enhance the ability to identify outstanding individual, at the same time reducing unnecessary or even erroneous redundancy, and finally make the algorithm could greatly reducing the amount of computation and further optimizing the planning results.

Then, the fitness function is further refined on the basis of the original fitness function; the fitness function model of the improved PIO algorithm is expressed as follows

$$\begin{aligned} Fitness(i) = {} & w_1 \cdot threat\_in(i) + w_2 \cdot threat\_out(i) \\ & + w_3 \cdot distance(i) + w_4 \cdot deviate(i) \end{aligned} \tag{17}$$

where $w_1 + w_2 + w_3 + w_4 = 1$.

When the following equation is satisfied in the R-parameter space

$$T_{center}(j) - T_{radius}(j) < \sigma_1^{i,k}(T) < T_{center}(j) + T_{radius}(j)$$

That is, the abscissa of the $k$th attitude node is within the threat region, $T_{center}$ and $T_{radius}$ are respectively the threat centers and threat radius; when the attitude node is located inside the threat sphere, as shown in Figure 5 where the fitness function of the $i$th individual relative to the $j$th threat region, then the fitness function is

$$threat\_in(\mathrm{i})^j = \begin{cases} 0 & \left|\sigma^i - T_j\right| > R_j \\ \frac{L_{i,j}}{5} \cdot t_j \left( \frac{1}{d_{0.1,j}^4} + \frac{1}{d_{0.3,j}^4} + \frac{1}{d_{0.5,j}^4} + \frac{1}{d_{0.7,j}^4} + \frac{1}{d_{0.9,j}^4} \right) & \left|\sigma^i - T_j\right| \leqslant R_j \end{cases} \tag{18}$$

If the attitude node only passes through the zone but does not enter the threat sphere, as shown in Figure 6 where the fitness function of the $i$th

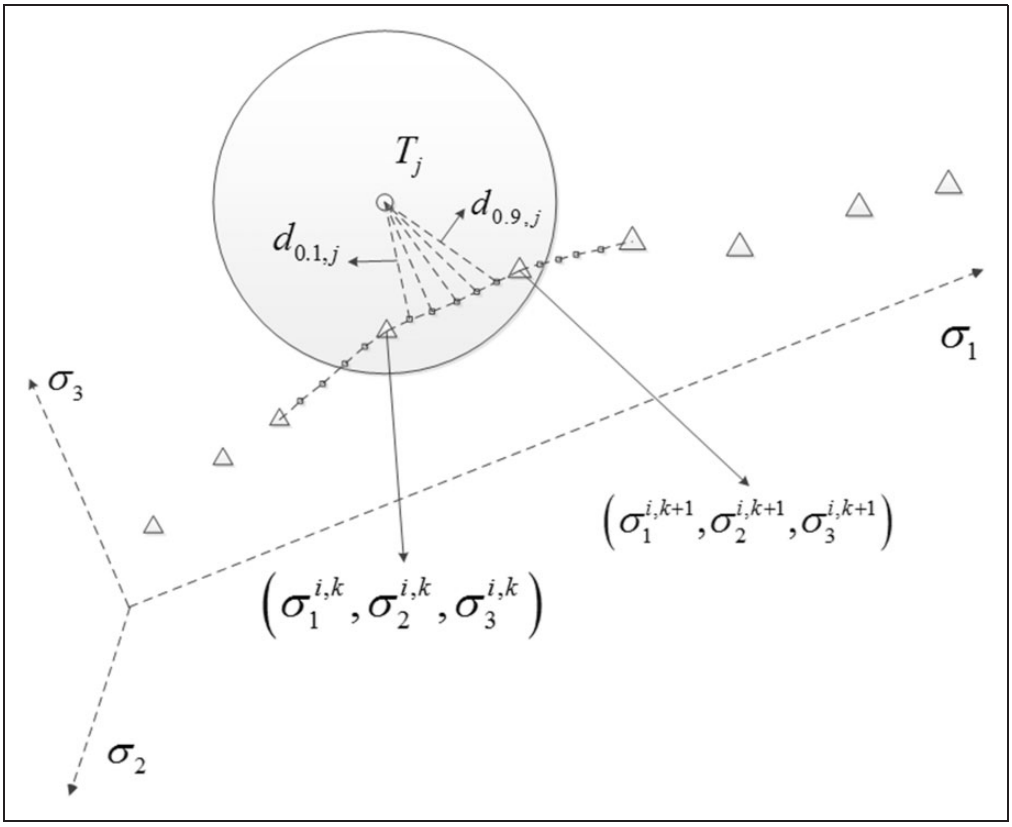


**Figure 5.** The attitude R-parameter entering the threat sphere.

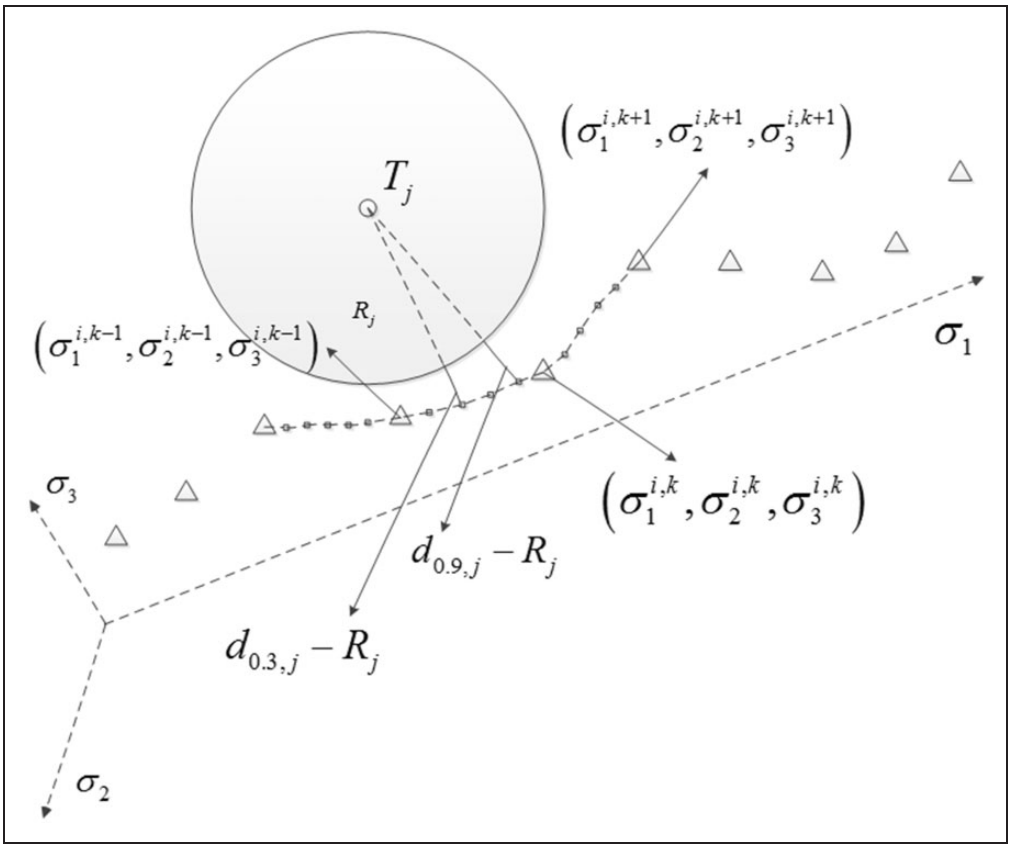


**Figure 6.** The attitude R-parameter which are not in the threat sphere.

individual relative to the $j$th threat region, the fitness function is

$$threat\_out(i)^j = \begin{cases} 0 & |\sigma^i - T_j| < R_j \\ t_j\left(\frac{1}{d_{0.1,j}^4 - R_j^4} + \frac{1}{d_{0.3,j}^4 - R_j^4} + \frac{1}{d_{0.5,j}^4 - R_j^4} + \frac{1}{d_{0.7,j}^4 - R_j^4} + \frac{1}{d_{0.9,j}^4 - R_j^4}\right) & |\sigma^i - T_j| \geqslant R_j \end{cases} \quad (19)$$

The overall distance cost of attitude planning is

$$diatance(i) = \sum_{j=0}^{n} L_{i,j} \quad (20)$$

The separation degree of the planning attitude R-parameter in the non-threat region with the optimal attitude planning is

$$deviate(k) = \begin{cases} 0 & MIN(T_{center}) < \sigma_1^{i,k}(T) < MAX(T_{center}) \\ \sqrt{\sigma_2^{i,k}(T) + \sigma_3^{i,k}(T)} & others \end{cases} \quad (21)$$

where $\sigma_1^{i,k}(T), \sigma_2^{i,k}(T), \sigma_3^{i,k}(T)$ denotes the $k$th R-parameter node of the $i$th individual in the $T$th iteration, $MIN(T_{center})$ and $MAX(T_{center})$ are the nearest and farthest threat centers from the origin in the R-parameter space. *threat_in* reflects the threat of attitude in the threat area, as the bound stable of the attitude is still an unstable state.

*threat_out* represents the margin of the attitude that does not enter the threat area, which is in the vicinity of a threat area. *deviate* represents the separation degree of the overall planning process from the optimal path of the target pose after it has departed the main threat area. The smaller value of *deviate* allows the planning process to quickly converge to the target attitude after leaving the threat region, *distance* is the summation of spacecraft fuel that is required for planning results.

## Improved PIO algorithm attitude planning process

*Attitude planning route.* Based on the attitude planning requirement and low detectable directivity requirements, combined with the ground, sea, space-based threat, satellite payload, and other attitude constraints model the model in the attitude space is transformed into the R-parameter space. Based on the corresponding initial attitude, the target pose, and the restricted region use improved PIO algorithm to output the attitude planning result as shown in Figure 7.

### Algorithm flow

1. Initialization parameters

The number of pigeons – $M$, the search dimension – $D$, initial attitude in R-parameter space – $\left[\sigma_{1,0} \quad \sigma_{2,0} \quad \sigma_{3,0}\right]^T$, map and compass operator iteration number – $T_1$, maximum number of iterations – $T_{MAX}$, R-parameter coordinates of the threat zone center – $T_{center}(k) = \left[\sigma_{1,T} \quad \sigma_{2,T} \quad \sigma_{3,T}\right]^T$, threat area radius –, threat level – $t_k$.

2. Initialize the position of the pigeon

By performing the map and compass operators according to equations (9) to (13), the number of iterations was considered to be $T_1$, and the local optimal $\sigma_p$ of each individual in the current iteration process was selected in each iteration process and the global optimal solution $\sigma_g$ was generated by all individuals during the current iteration process. The fitness values of each iteration were calculated, and if the fitness value changing rate was less than the threshold value, the activation factor was found to be less than three times, and if the fitness value of the activation factor that started-up before was continuously decreased, then it initiated the activation factor iteration by 30 times.

3. Perform the landmark operator

According to equation (7) to carry on the evolution, the center of the current population was calculated according to equation (8) in each iteration, and

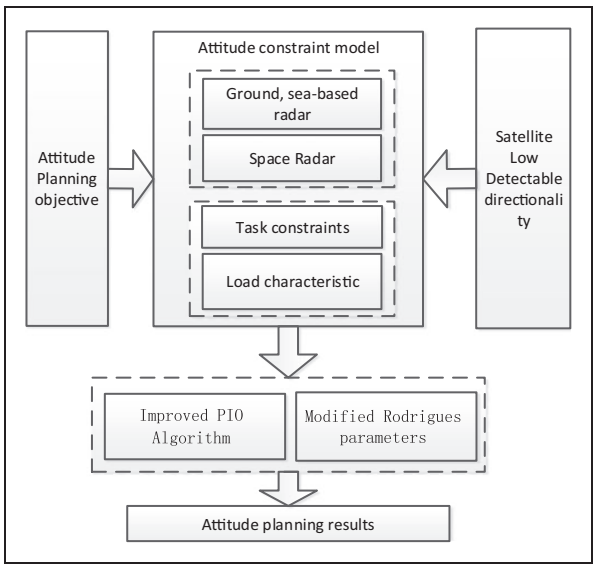


**Figure 7.** The overall structure of the algorithm. PIO: pigeon-inspired optimization.

ranked all individuals according to the fitness value, and exclude half of the individuals away from the center, when the iteration count reaches $T_{MAX}$, the output of the planning result would be present as shown in Figure 8.

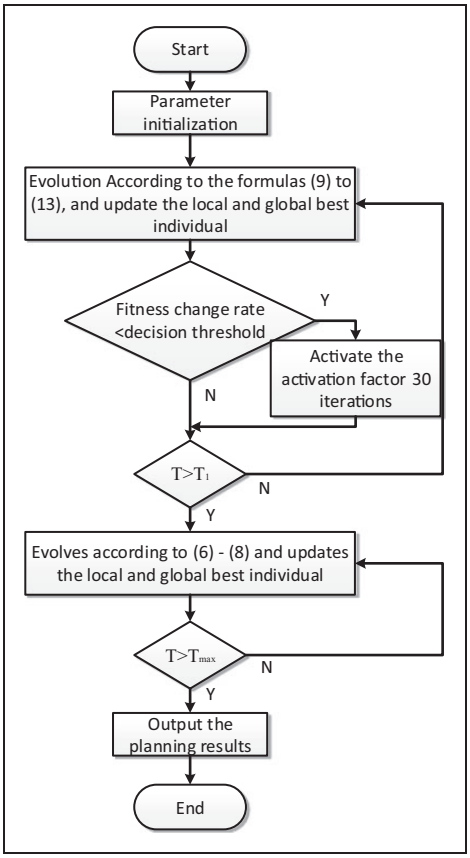


**Figure 8.** Flow chart of improved PIO algorithm.

## Experimental results

Considering the satellites according to the direction of ground, sea-, and space-based radar threat, the pitch, roll, and yaw angles need to be set to 67.1/78°, 34.2033°, and 89.1149°, respectively. And according to the CCD camera lens carried by the satellite, it has to avoid the sun in an angle range of exposure, as well as in response to the monitoring of space optical detection.

Satellites carrying payloads of identifiable payload shall not appear within the field of view of optical monitoring satellites, and the visible payload carried by the satellite cannot be seen in the field of view of the optical monitoring satellite, etc. In accordance with the constraints on satellite attitude, assuming that the satellite attitude in the planning process has to avoid five attitude-restricted areas, these regional centers would be: (30.0686°, 41.0227°, 59.9134°), (20.2542°, 25.8577°, 13.8438°), (44.6379°, 53.2570°, 66.8640°), (27.9892°, 18.5119°, 44.2494°), (57.4206°, 43.1903°, 72.9207°), and based on the size of the restrictive attitude range and the threat level, the radius of five threat regions are set as: 10°, 10°, 8°, 12°, 8°and the threat levels are: 12, 8, 14, 5, 10.

The experimental conditions are quad-core 2.4 GHz, 6 GB memory, 64-bit computer, and the internal parameters of the algorithm are as follows.

- Classic PIO algorithm:

The number of individuals is $M = 30$, the planning dimension $D = 20$, and the number of

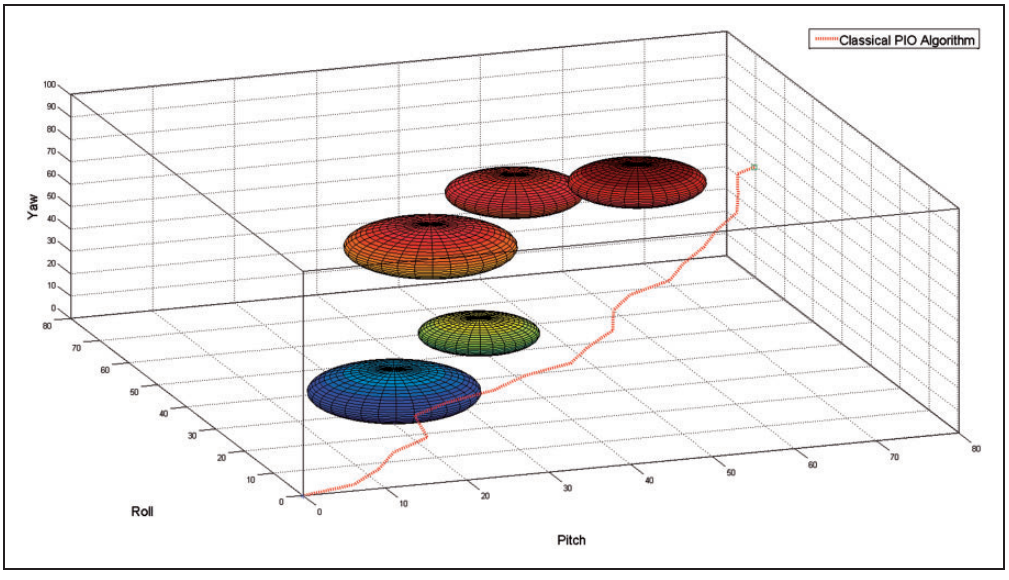


**Figure 9.** Planning results with $D = 20$, $M = 30$, $T_{MAX} = 200$.
PIO: pigeon-inspired optimization.

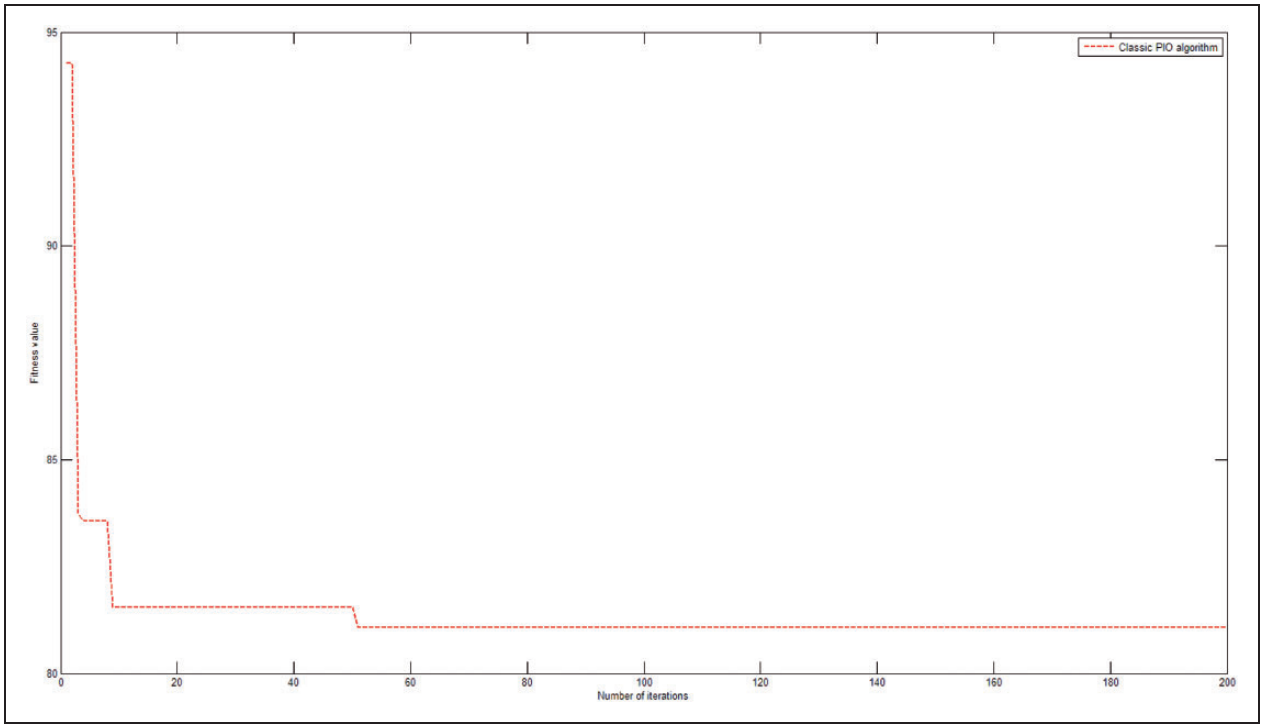


**Figure 10.** The change of fitness with $D = 20$, $M = 30$, $T_{MAX} = 200$.

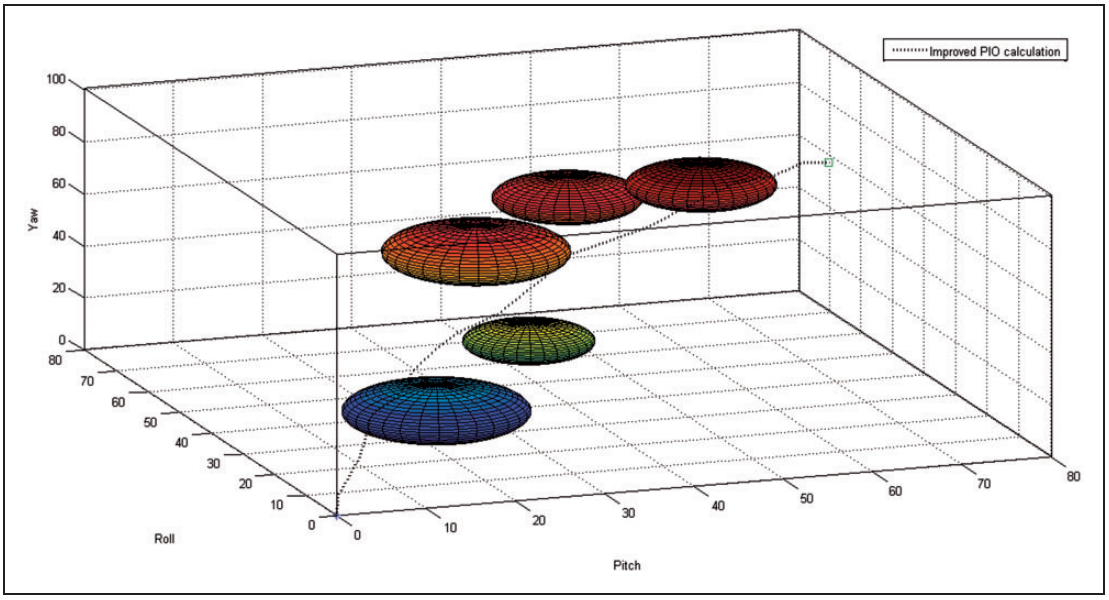


**Figure 11.** Planning results for $D = 20$, $M = 30$, $T_{MAX} = 200$.
PIO: improved pigeon-inspired optimization.

iterations is 200 as shown in Figure 9 and Figure 10 (map and compass operator 150 times, landmark operator 50 times).

- Improved PIO algorithm:
  1. The number of individuals $M = 30$, the planning dimension as shown in Figure 11, Figure 12 and Figure 17 $D = 20$, the number of iterations 200 times (map and compass operator 150 times, landmark operator 50 times);
  2. The number of individuals $M = 30$, the planning dimension $D = 20$, the number of iterations 400 times as shown in Figure 13 and

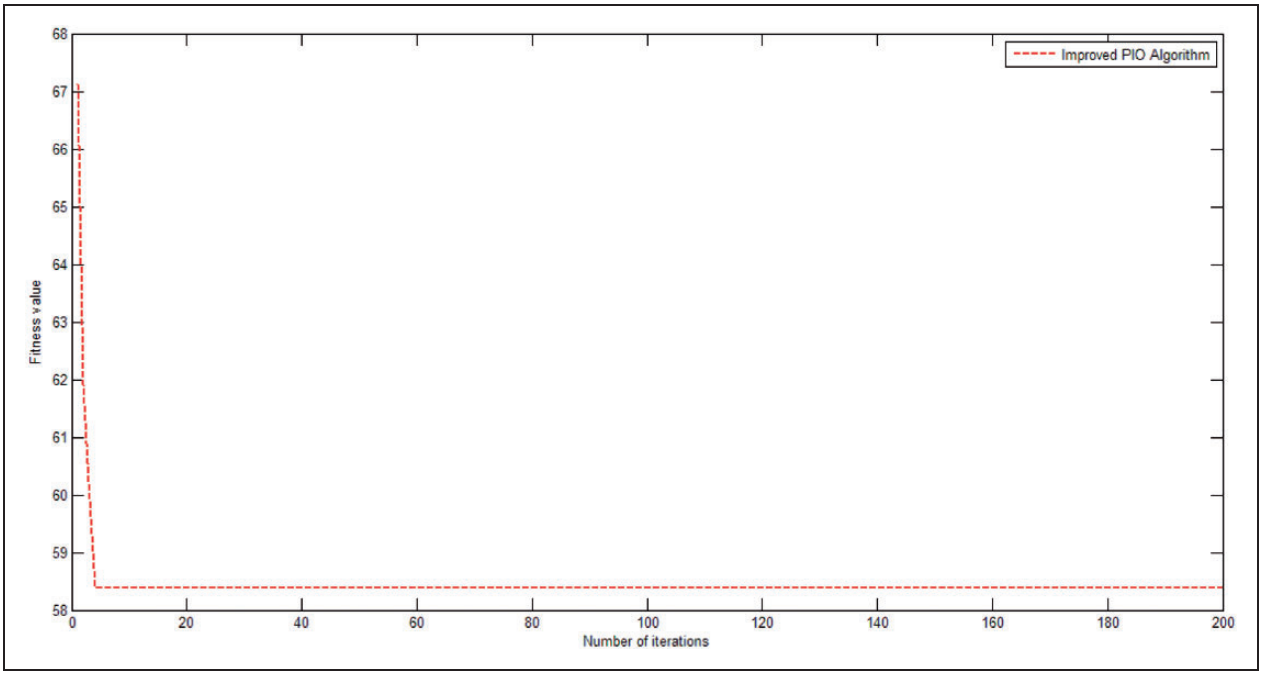


**Figure 12.** The change of fitness with $D = 20$, $M = 30$, $T_{MAX} = 200$.
PIO: improved pigeon-inspired optimization.

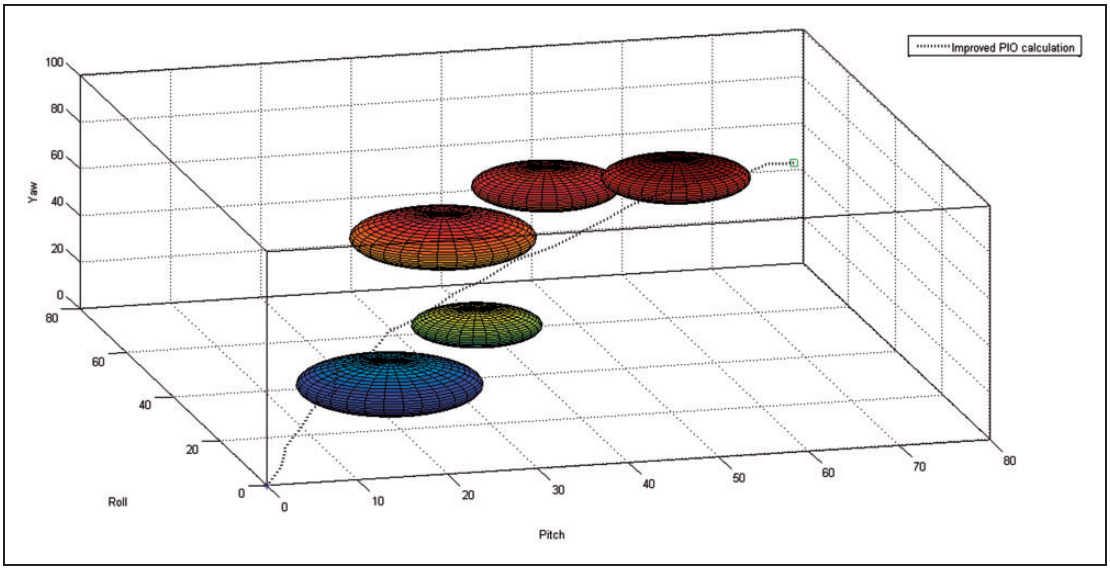


**Figure 13.** Planning results for $D = 20$, $M = 30$, $T_{MAX} = 400$.
PIO: improved pigeon-inspired optimization.

Figure 14 (map and compass operator 350 times, the landmark operator 50 times);

3. The number of individuals $M = 60$, the planning dimension $D = 20$, the number of iterations 400 times as shown in Figure 15 and Figure 16 (map and compass operator 350 times, the landmark operator 50 times).
4. A relative complex example:

Set the target attitude angle to 67.1078°, 56.2037°, 72.1149°, restricted areas increase to 10 groups, respectively: (45.0685°, 35.0226°, 59.931417°), (20.2542°, 25.8576°, 23.8438°), (63.6379°, 23.2570°, 78.8640°), (34.9892°, 18.5119°, 34.2494°), (57.4206°, 37.1903°, 72.9206°), (50°, 30°, 45°), (65°, 55°, 50°), (25°, 10°, 25°), (30°, 35°, 50°), (42°, 14°, 65°). Its corresponding threat area radiuses are 10°, 10°, 8°, 7°, 8°,

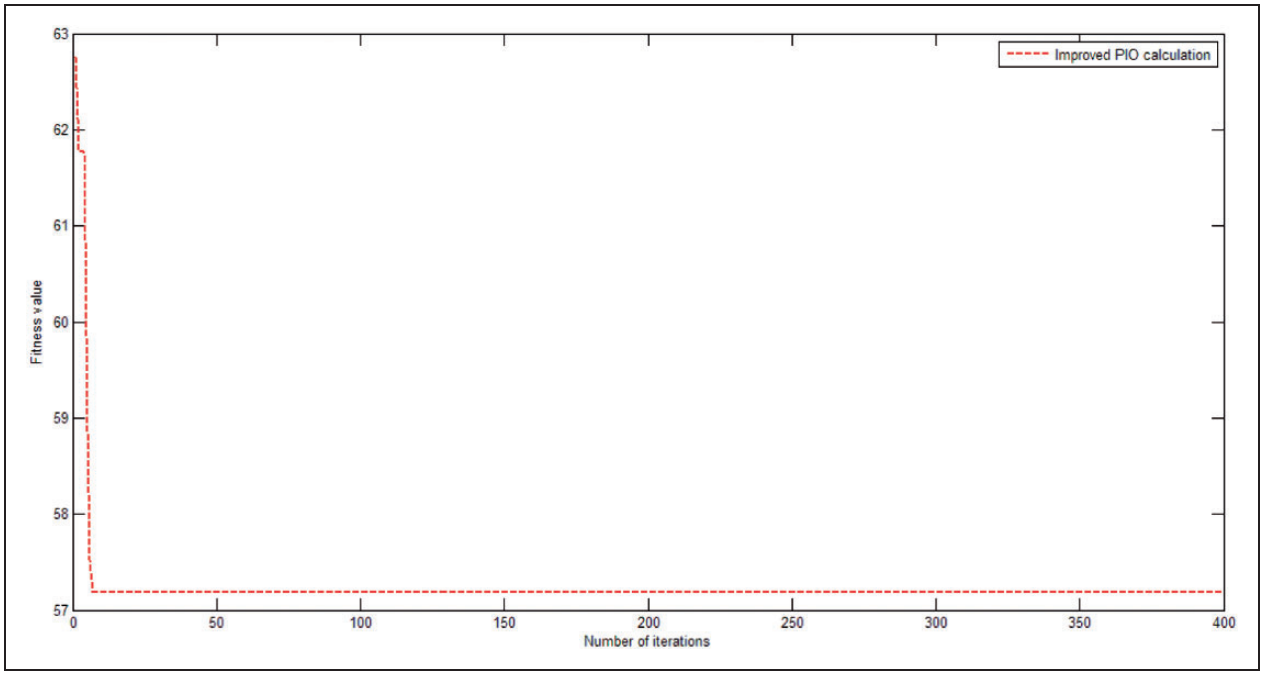


**Figure 14.** The change of fitness with $D = 20$, $M = 30$, $T_{MAX} = 400$.
PIO: improved pigeon-inspired optimization.

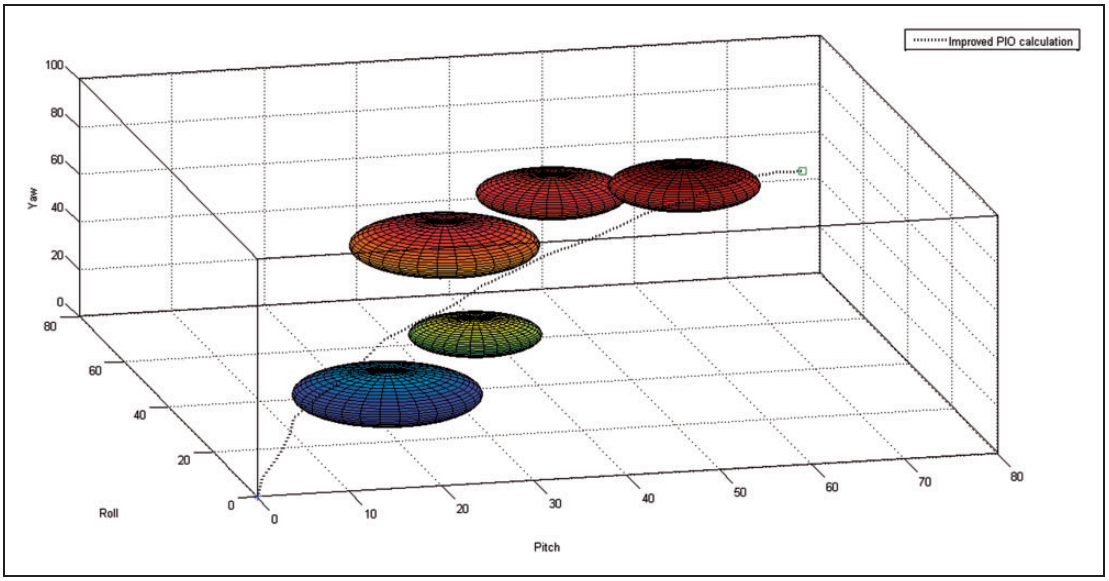


**Figure 15.** Planning results for $D = 20$, $M = 60$, $T_{MAX} = 400$.

7°, 9°, 8°, 9°, 8°. Corresponding threat levels are 15, 18, 10, 25, 16, 18, 17, 25, 7, 8 as shown in Figure 18, Figure 19 and Figure 20.

### *Classic PIO algorithm planning results*

The operation time at $D = 20$, $M = 30$, $T_{MAX} = 200$ is shown in Table 1.

### *Improved PIO algorithm planning results*

The following results can be drawn from simulation:

1. Convergence speed: Compared with 50 iterations of the classical PIO algorithm, the improved PIO algorithm has faster convergence speed, and can find the global optimal solution at the fourth iteration.

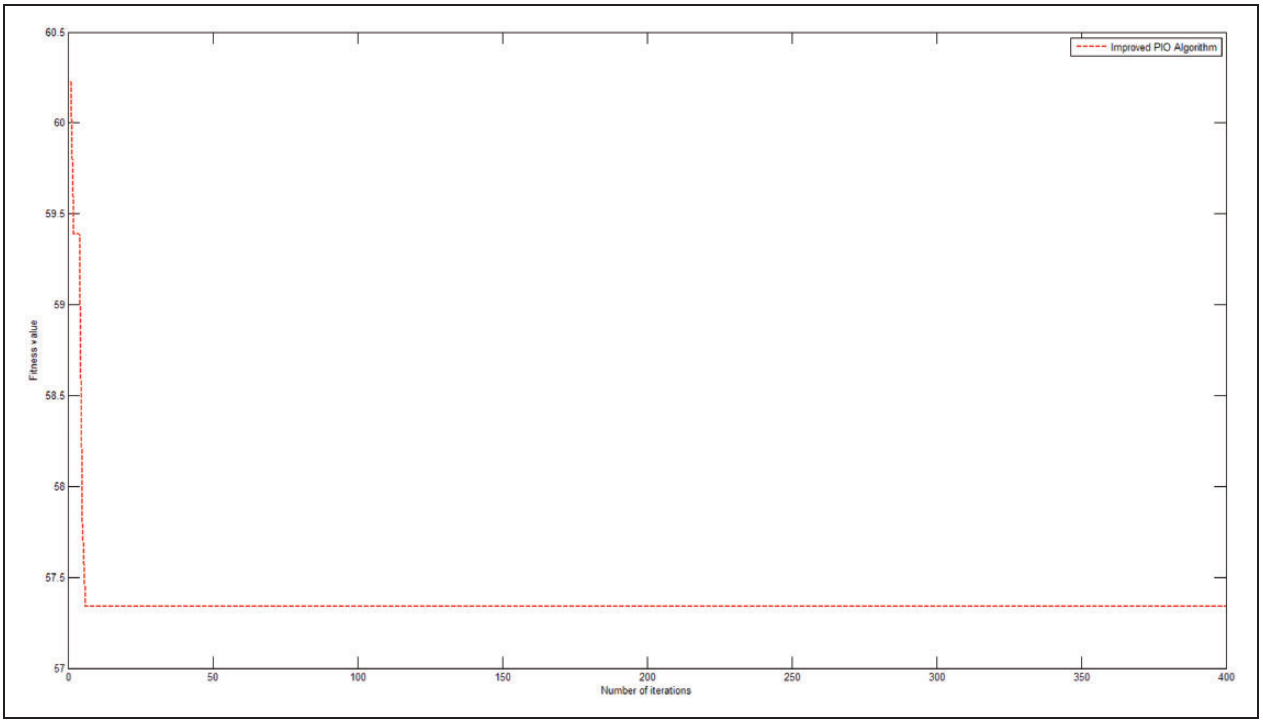


**Figure 16.** The change of fitness with $D = 20$, $M = 60$, $T_{MAX} = 400$.

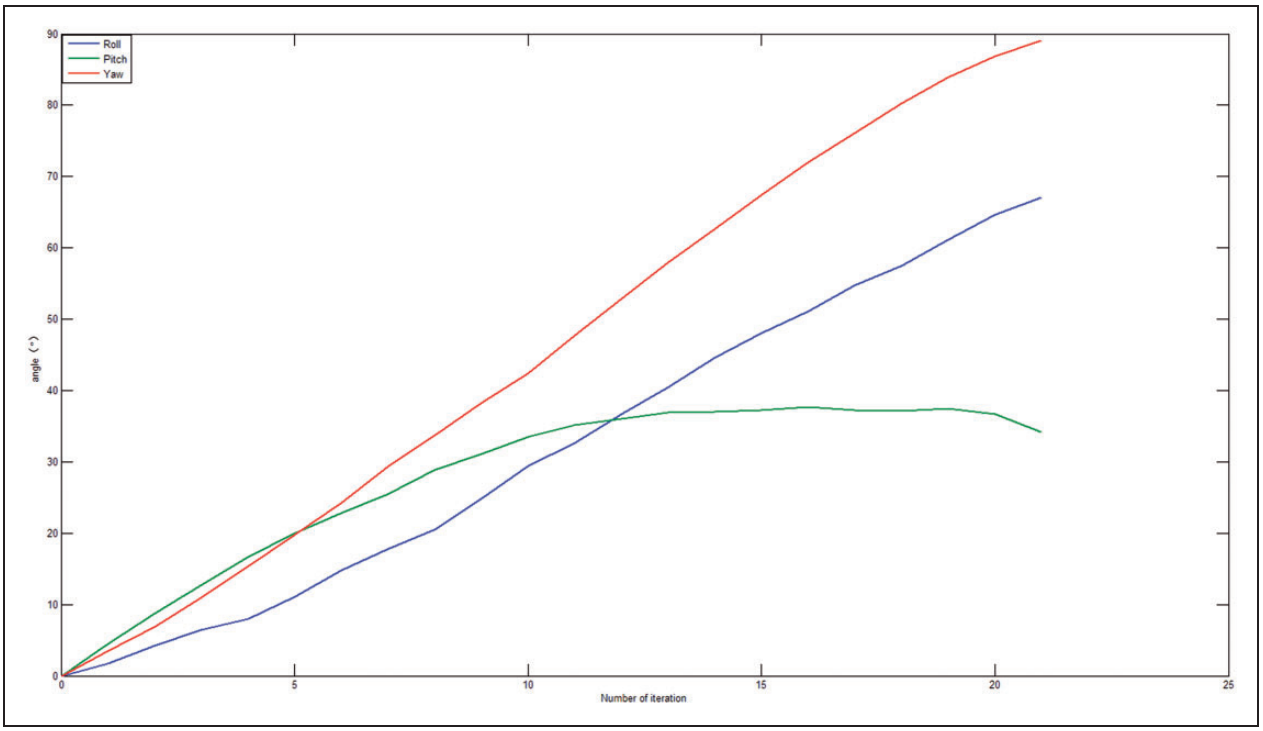


**Figure 17.** Three-axis attitude planning results.

2. CPU resource consumption: Based on the same model parameters, initial conditions, and constraints, the operating time of the classical PIO algorithm is 120.630 s, the improved PIO algorithm is 20.621 s, and the modified algorithm does not need cross-product, which reduces the computational complexity to a great extent and realizes the optimization of the algorithm.
3. Planning result: From the planning result image, the improved PIO algorithm can smoothen the

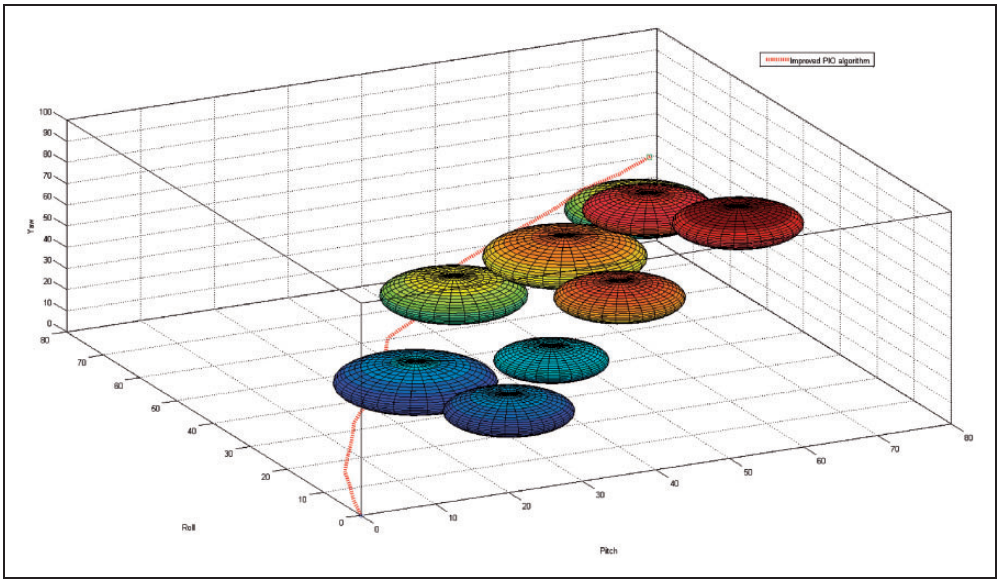


**Figure 18.** Planning result for $D = 20$, $M = 30$, $T_{MAX} = 200$.
PIO: improved pigeon-inspired optimization.

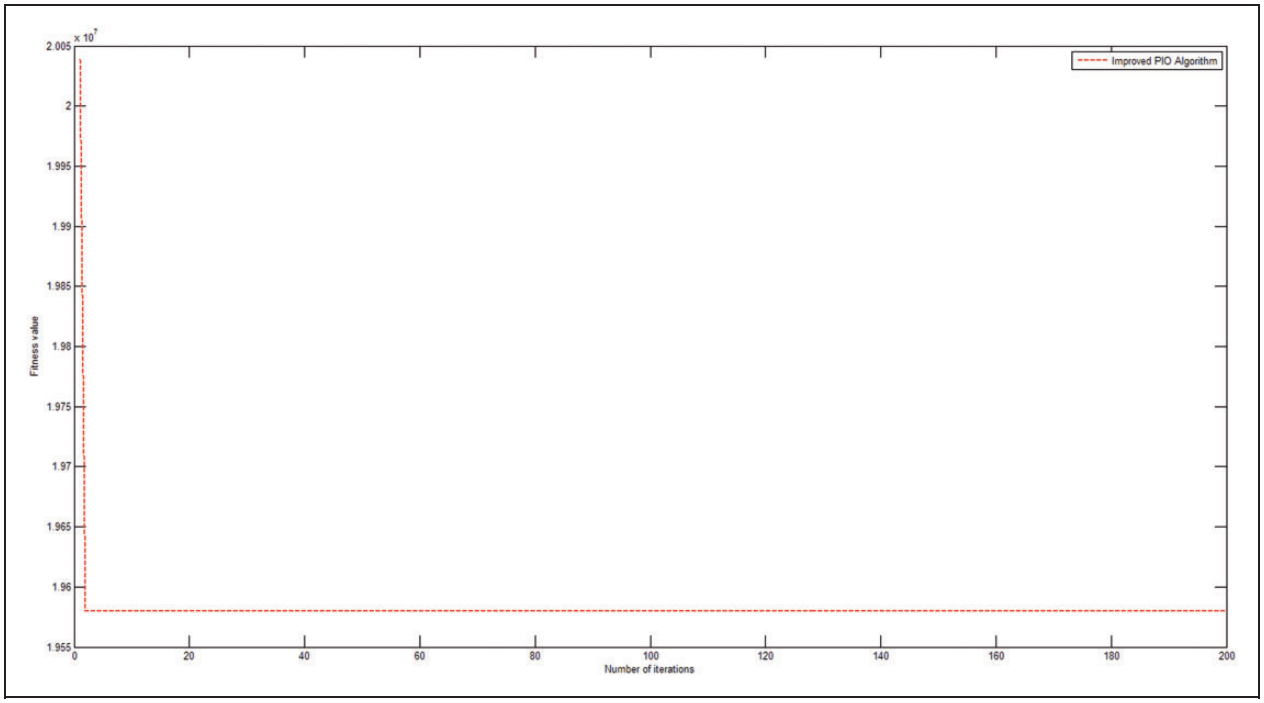


**Figure 19.** The change of fitness with $D = 20$, $M = 30$, $T_{MAX} = 200$.
PIO: improved pigeon-inspired optimization.

planning result curve, and reduce the unnecessary attitude adjustment and jitter to a great extent.

Based on the above three points, it can be seen that compared to the classic PIO algorithm and its fitness function, the improved PIO algorithm achieves a significant improvement in the convergence speed, CPU resource consumption, and planning results, and achieves the optimization of the attitude planning as shown in Table 2.

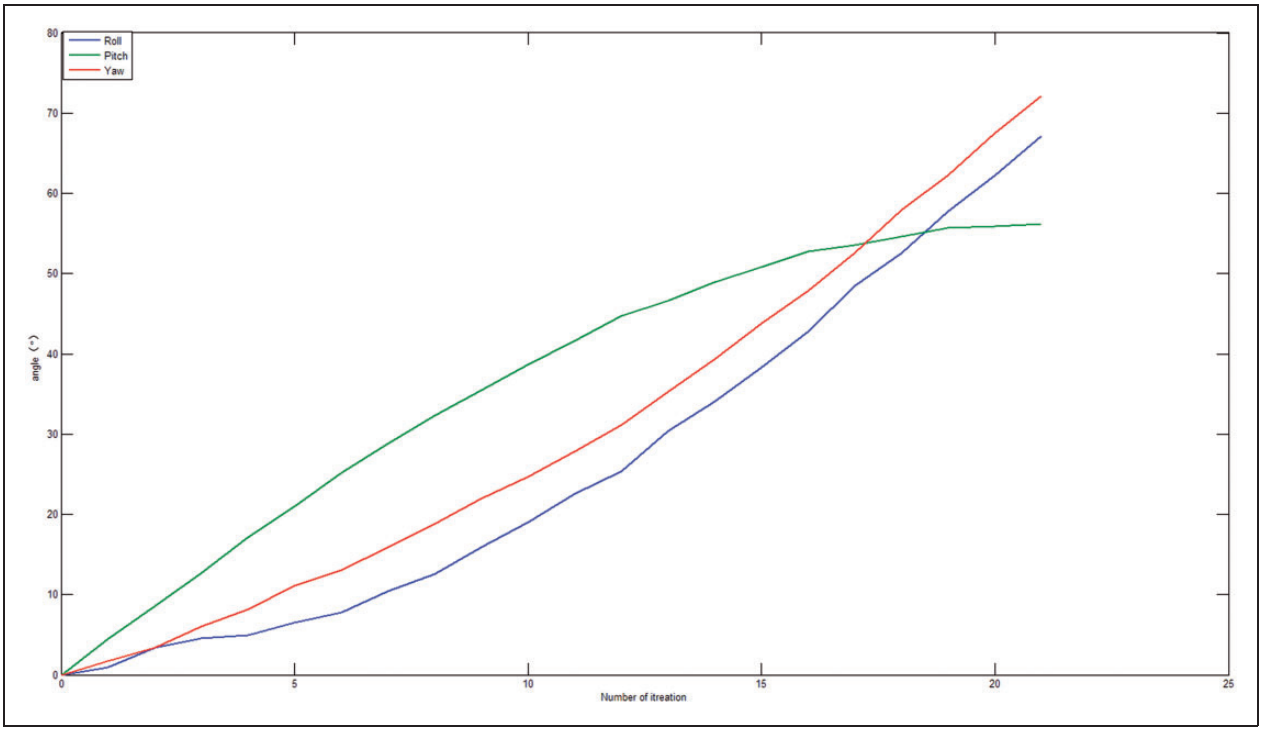


**Figure 20.** Three-axis attitude planning results.

**Table 1.** Operating time of the classical pigeon-inspired optimization (PIO) algorithm when $D = 20$, $M = 30$, $T_{MAX} = 200$.

| Function name | Number of calls | Total time (s) | Own time (s) |
|---|---|---|---|
| Main program | 1 | 120.630 | 1.654 |
| PIO algorithm | 1 | 116.090 | 1.162 |
| Fitness value calculation function | 10,463 | 114.850 | 69.462 |
| Distance calculation function | 4,557,137 | 29.967 | 29.967 |
| cross-product | 1,098,615 | 15.421 | 15.421 |

PIO: pigeon-inspired optimization.

**Table 2.** Operating time of the improved pigeon-inspired optimization (PIO) algorithm when $D = 20$, $M = 30$, $T_{MAX} = 200$.

| Function name | Number of calls | Total time (s) | Own time (s) |
|---|---|---|---|
| Main program | 1 | 20.621 | 0.236 |
| PIO algorithm | 1 | 19.094 | 0.374 |
| Fitness value calculation function | 10,463 | 18.654 | 9.812 |
| Distance calculation function | 1,216,716 | 8.841 | 8.841 |
| cross-product | 0 | 0 | 0 |

## Conclusion

In this paper, microsatellites under the conditions of payload, space mission to attitude complex constraints are considered, and in order for the satellite to achieve low detectability of the earth, sea, and space-based detection equipment, an improved PIO optimal algorithm based on modified Rodrigues parameter space is designed, which is quite different when compared to the classic PIO algorithm. The improved PIO algorithm has significant improvement in planning results, on-board control system resources, algorithm convergence speed, so that satellites in conjunction with low RCS structure, materials, and coating design for different wavelengths of radar, infrared, and optical detection equipment maintain low detectability. Even in the threat device detection area, reasonably set attitude constraints can hide the satellite payload so as to achieve the purpose of hiding or deceiving detection equipment.

### Declaration of Conflicting Interests

The author(s) declared no potential conflicts of interest with respect to the research, authorship, and/or publication of this article.

### Funding

The author(s) received no financial support for the research, authorship, and/or publication of this article.

## References


1. Cao XY. New Development of the United States space surveillance system. *Aerosp China* 2010; 4: 32–35.
2. Huo ML, Mu YM and Peng H. Direction and implication of the development of the U.S. Anti-Satellite Weapons. *Natl Defens Sci Technol* 2013; 34: 22–26.
3. Li Y and Kang KH. Research and analysis on development of US Space Based Surveillance System. *Spacecraft Eng* 2008; 17: 76–82.
4. Qiao K, Wang ZL and Cong MY. Analysis on space based and ground based surveillance system to space target. *Optic Techniq* 2006; 32: 744–749.
5. Su K and Zhou JJ. Flight attitude planning for low observable micro-satellite shields. *Acta Aeronaut Astronaut Sin* 2011; 32: 720–728.
6. Singh G, Macala G, Edward C, et al. A constraint monitor algorithm for the Cassini spacecraft. In: *Proceedings of AAIA guidance, navigation and control conference*, Washington D.C., USA, 1997, pp.272–282.
7. McInnes CR. Large angle slew maneuvers with autonomous sun vector avoidance. *J Guid Control Dyn* 1994; 17: 875–877.
8. Avanzini G, Radice G and Ali I. Potential approach for constrained autonomous of a spacecraft equipped with a cluster of control moment gyroscopes. *Proc IMechE, Part G: J Aerospace Engineering* 2009; 223: 285–296.
9. Kim Y and Mesbahi M. Quadratically constrained attitude control via semidefinite programming. *IEEE Trans Autom Control* 2004; 49: 731–735.
10. Su K and Zhou JJ. Real-time attitude planning for low RCS micro-satellites with limited attitude control ability. *Acta Aeronaut Astronaut Sin* 2010; 30: 1841–1848.
11. Wang Y and Han CX. Overview of American Space Fence. *Mod Radar* 2014; 36: 16–18.
12. Zhou JH, Miao YH and Wang HM. Attitude representation using Rodrigues parameter. *J Astronaut* 2004; 25: 514–519.
13. Zhao CS, Qin YY, Jia JC, et al. Research on the modified Rodrigues parameters based attitude algorithm. *Meas Control Technol* 2009; 28.
14. Duan HB and Qiao PX. Pigeon-inspired optimization: a new swarm intelligence optimizer for air robot path planning. *IJICC* 2014; 7: 24–37.
15. Zhang SJ and Duan HB. Gaussian pigeon-inspired optimization approach to orbital spacecraft formation reconfiguration. *Chinese J Aeronaut* 2015; 28: 200–205.
16. Li C and Duan HB. Target detection approach for UAVs via improved pigeon-inspired optimization and edge potential function. *Aerosp Sci Technol* 2014; 39: 352–360.
17. Bo Z and Duan HB. Three-dimensional path planning for uninhabited combat aerial vehicle based on predator-prey pigeon-inspired optimization in dynamic environment. In: *IEEE/ACM Trans Comput Biol Bioinform* 2015; DOI: 10.1109/TCBB.2015.2443789.
18. Sun CH, Duan HB and Shi YH. Optimal satellite formation reconfiguration based on closed-loop brain storm optimization. *IEEE Comput Intell Mag* 2013; 8: 39–51.
19. Zhong GW, Cui YP and Cui GT. Autonomous attitude maneuver planning for spacecraft under complex constraints. *Acta Aeronaut Astronaut Sin* 2007; 28: 1091–1097.
20. Ding XD, Liu Y and Li WM. Dynamic RCS and real-time based analysis of method of UAV route planning. *Syst Eng Electron* 2008; 30: 867–871.
21. Zhang RW. *Satellite orbit attitude dynamics and control*. Beijing: Beihang University Press, 1998.


# Appendix

## Notation

| | |
|---|---|
| $d_{0.1,k}$ | distance from the $k$th threat center to one-tenth of this planning segment |
| *deviate* | separation degree of the overall planning process |
| *distance* | summation of the spacecraft fuel required for planning results |
| $D$ | individual evolution dimension |
| $e_1$ | individual factor |
| $e_2$ | communication factor |
| $Fitness(X_i(T))$ | fitness value of the $i$th individual in the $T$th evolution |
| *inv* | absolute value function of a normal distribution with the mean of 0 and the variance of $\varepsilon$ |
| $L_{i,j}$ | length of the $j$th planning segment of the $i$th individual |
| $M$ | number of individuals |
| $M(T)$ | number of individuals in the $T$th evolution |
| $\mathrm{MIN}(T_{center})$ | nearest and farthest threat |
| $\mathrm{MAX}(T_{center})$ | centers from the origin |
| $N_t$ | number of threats |
| *rand* | a random number between 0 and 1 |
| $R$ | map compass factor |
| $R_j$ | threat radius of the $j$th threat |
| $R_{i,j}$ | mean distance from the $i$th planning segment to the $j$th threat center |
| $t_k$ | threat level of the $k$th threat |
| *threat_in* | threat of attitude which is in the threat area |
| $threat\_in(i)^j$ | when attitude node is located inside the $j$th threat sphere |
| *threat_out* | margin of the attitude that does not enter the threat area |
| $threat\_out(i)^j$ | attitude node only does not enter the $j$th threat sphere |
| $T$ | current number of iterations |
| $T_1$ | number of iterations of the map compass operator |
| $T_{\mathrm{MAX}}$ | maximum number of iterations |
| $T_{center}(k)$ | No. of $k$ centers of the threat region |
| $T_{radius}(k)$ | No. of $k$ radiuses of the threat |
| $V(T),\sigma(T)$ | R-parameter representation of the three-axis angle and angular velocity of the satellite evolved in the $T$th iteration |
| $w_1,w_2,w_3,w_4$ | weight coefficients |

| | |
|---|---|
| $x_i, v_i$ | position and velocity of the $i$th individual |
| $x_p, x_g$ | optimal positions for each individual in the current iteration |
| $X_C(T)$ | position of the current pigeons center |
| $\varepsilon$ | variance of $inv$ |
| $\gamma$ | roll |
| $\psi$ | yaw |
| $\Phi$ | modified Rodrigues parameter |
| $\sigma_g$ | global optimal evolution result of all individuals before the current iteration |
| $\sigma_p$ | local optimal evolution results of the individual before the current iteration |
| $\sigma^i(T)$ | R-parameter of the satellite attitude angle evolved by the $i$th individual in $T$th iteration |
| $\sigma_1^{i,k}(T)$ | abscissa of the $k$th attitude node is within the threat region |
| $\sigma_1^{i,k}(T)$, $\sigma_2^{i,k}(T), \sigma_3^{i,k}(T)$ | $k$th R- parameter node of the $i$th individual in the $T$th iteration |
| $\theta$ | pitch |